

---

# THE eXTREME MESH DEFORMATION APPROACH (X-MESH) FOR THE STEFAN PHASE-CHANGE MODEL

---

arXiv PRE-PRINT

**Nicolas Moës**

Ecole Centrale de Nantes  
GeM Institute, UMR CNRS 6183  
Institut Universitaire de France (IUF)  
1 rue de la Noë, 44321 Nantes, France  
nicolas.moes@ec-nantes.fr

**Jean-François Remacle**

Université Catholique de Louvain  
Institute of Mechanics, Materials and Civil Engineering  
1348 Louvain-la-Neuve, Belgium  
jean-francois.remacle@uclouvain.be

**Jonathan Lambrechts**

Université Catholique de Louvain  
Institute of Mechanics, Materials and Civil Engineering  
1348 Louvain-la-Neuve, Belgium  
jonathan.lambrechts@uclouvain.be

**Benoît Lé**

Ecole Centrale de Nantes  
GeM Institute, UMR CNRS 6183  
1 rue de la Noë, 44321 Nantes, France  
benoit.le@ec-nantes.fr

November 9, 2021

## ABSTRACT

The eXtreme MESH deformation approach is a new method to follow sharp interfaces without remeshing and without changing the mesh topology. Moreover, the interface may change topology (nucleation, coalescence, splitting). The key idea is to allow elements to reach zero measure. This permits interface relaying, annihilation and seeding in a time continuous manner. The paper targets the Stefan phase-change model. Several examples demonstrate the capability of the approach.

**Keywords** X-MESH, Front relaying, Sharp interface, Phase-change

## 1 Introduction

The Stefan model is a classical phase-change model in which motion is neglected: fluid and solid are at rest (and expansion due to freezing is neglected). The phase-change takes place at a given temperature (0 degrees Celsius for water-ice) and the free energy is continuous across the front. The internal energy on the contrary is discontinuous and the jump gives the amount energy (latent heat) released by the fluid as it becomes solid. The heat flux is also discontinuous across the front, it is equal to the product of the latent heat times the front velocity.

The Stefan model leads to a stable solidification process because surface tension and kinetic mobility are neglected Jaafar et al. [2017]. To model unstable processes as dendritic growth, the fixed front temperature must be replaced by the so-called Gibbs-Thomson condition. This relation links the front temperature to a reference melting temperature, the front curvature and the front speed. There also exist anisotropic versions of the Gibbs-Thomson which take into account the local orientation of the interface surface. It influences the both the surface tension and kinetic mobility. For a flat front with very slow motion, the classical front temperature (273.15 Kelvin) is recovered.

As an illustration, consider Figure 1: the Stefan phase change model for the freezing of water (or melting of ice). The liquid occupies the region  $0 \leq x < \infty$ . We look for a temperature field  $T(x, t)$  that is initially at a temperature,  $T(x, 0) = T_h > T_0$  where  $T_0$  is the temperature of phase transition. For all  $t > 0$ , the left side  $x = 0$  of the domain is cooled:  $T(0, t) = T_c < T_0$ . Solidification begins immediately and the solid phase occupies a region  $0 \leq x \leq x_I(t)$  where  $x_I(t)$  is the position of the interface at time  $t$ :  $T(x_I(t), t) = T_0$ . Figure 1 shows the solution  $T(x, t)$  for physically sound ice and water parameters ( $T$  is in Celsius so  $T_0 = 0$ ). Even though  $T(x, t)$  is continuous, both time

and space derivatives  $d_t T(x_I(t), t)$  and  $d_x T(x, t_I(x))$  are discontinuous across the front. Their jumps are linked with the interface velocity to ensure temperature continuity.

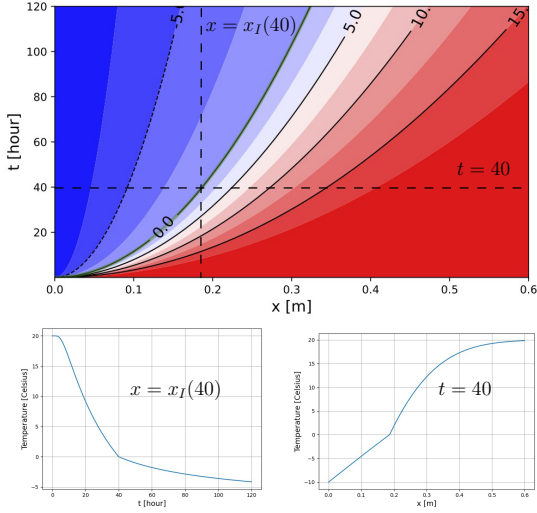


Figure 1: Temperature field for a Stefan problem.

Numerical schemes to address the Stefan model may be classified in tracking approaches or capturing approaches. In the first category, the mesh moves with the interface. This is the case for the Arbitrary Eulerian Lagrangian approach Baines et al. [2009], Gros et al. [2018], Zhang et al. [2019]. Unfortunately ALE is not able to handle topological changes of the front and requires remeshing when the mesh is too distorted. Remeshing requires projection of the solution from one mesh to the another which is highly detrimental to the continuity of the solution in time. Capturing approaches use a fixed mesh. This is the case for the level set approach Chen et al. [1997], Shaikh et al. [2016] and the extended finite element method Merle and Dolbow [2002], Ji et al. [2002], He et al. [2021].

We consider in this paper a new paradigm for mesh movements allowing elements to reach zero measure at some instant in their evolution. This extreme mesh deformation (X-MESH) allows an interface to be relayed from one node to the another node in a continuous fashion. It also allows interface annihilation or seeding. Moreover, no remeshing is needed and the mesh topology can be kept fixed. Only mesh movements are needed.

The paper is organized as follows. Section 2 describes the equation of the Stefan model both in strong and weak form, as

well as the temperature update procedure. Section 3 describes the front relaying process by the X-MESH approach. A staggered scheme is described in section 4 that iterates between the temperature update and the mesh update. A semi-monolithic is also described in section 5. In Section 6, a set of 2D simulations are presented, some for a zero latent heat and some for a non-zero latent heat. Both the staggered and semi-monolithic schemes are tested.

## 2 Two-phase Stefan model

### 2.1 Continuous problem

We consider a domain  $\Omega$  depicted in figure 2, with boundaries  $\partial\Omega$  which are fixed in time, divided into two domains  $\Omega_s$ , which corresponds to the solid phase, and  $\Omega_\ell$  which corresponds to the liquid phase. In the context of phase-change modelling, the boundary  $\Gamma$  between these two domains may move at a speed  $w$  with respect to the time  $t$ .

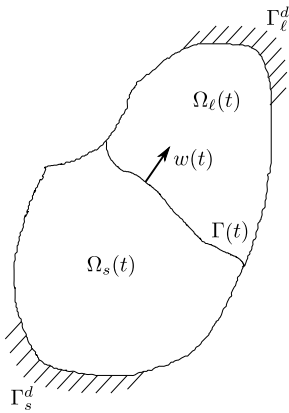


Figure 2: Problem definition.

We seek to determine the evolution of the temperature field  $T(\mathbf{x}, t)$  [K] for  $(\mathbf{x}, t) \in \Omega \times [0, T_{\max}]$ , which satisfies the governing equations

$$\rho_s c_s T_{,t} = \nabla \cdot (k_s \nabla T) + \rho_s S \text{ in } \Omega_s \quad (1a)$$

$$\rho_\ell c_\ell T_{,t} = \nabla \cdot (k_\ell \nabla T) + \rho_\ell S \text{ in } \Omega_\ell \quad (1b)$$

where  $\rho_s$  and  $\rho_\ell$  are the volumic masses [ $\text{kg} \cdot \text{m}^{-3}$ ],  $c_s$  and  $c_\ell$  the specific heat capacities [ $\text{J} \cdot \text{K}^{-1} \cdot \text{kg}^{-1}$ ],  $k_s$  and  $k_\ell$  the conductivities [ $\text{W} \cdot \text{m}^{-1} \cdot \text{K}^{-1}$ ] of the phases and  $S$  a heat source [ $\text{W} \cdot \text{kg}^{-1}$ ]. We consider without loss of generality isotropic conductivities.

To ensure mass conservation with the Stefan model, the volumic mass must be considered uniform, so  $\rho_s = \rho_\ell = \rho$ . The temperature field must satisfy the following boundary and initial conditions

$$T(\mathbf{x}, t) = T_d \text{ if } \mathbf{x} \in \Gamma^d \quad (2a)$$

$$T(\mathbf{x}, t) = T_0 \text{ if } \mathbf{x} \in \Gamma(t) \quad (2b)$$

$$T(\mathbf{x}, 0) = T_i \text{ on } \Omega \quad (2c)$$

Here,  $T_d$  is the temperature imposed on the Dirichlet boundary  $\Gamma^d = \Gamma_s^d \cup \Gamma_\ell^d$ . On the phase change front  $\Gamma$ , the heat flux jump is related to the front speed by

$$(k_s \nabla T - k_\ell \nabla T) \cdot \mathbf{n} = \rho \ell (\mathbf{w} \cdot \mathbf{n}) \quad (3)$$

where  $\mathbf{n}$  is the normal to  $\Gamma(t)$  and  $\ell$  is the latent heat [J.K<sup>-1</sup>].

The strong form of the equations as written just above are equivalent to the following variational problem: find  $T \in \mathcal{U}$  such that for  $t \in [0, T_{\max}]$ ,

$$\begin{aligned} & \frac{d}{dt} \int_{\Omega(t)} \rho e(T) T^* \, d\Omega + \int_{\Omega(t)} k \nabla T \cdot \nabla T^* \, d\Omega \\ & - \int_{\Omega(t)} \nabla \cdot (\rho e(T) \mathbf{w}) T^* \, d\Omega - \int_{\Gamma(t)} [\rho e(T)] \mathbf{w} \cdot \mathbf{n} T^* \, d\Gamma = \int_{\Omega(t)} \rho S T^* \, d\Omega, \quad \forall T^* \in \mathcal{U}_0 \end{aligned} \quad (4)$$

Function spaces where lives both the temperature  $T$  and test function  $T^*$  are defined as

$$\mathcal{U} = \{T \in H(\Omega(t)), \quad T = T_d \text{ on } \Gamma^d\} \text{ and } \mathcal{U}_0 = \{T \in H(\Omega(t)), \quad T = 0 \text{ on } T_d\}.$$

Note here that one essential condition (2b) is not a priori satisfied by  $T$  but its imposition will be done through the solution and mesh update process.

The free energy expression is given by:

$$\rho e(T) = \begin{cases} \rho c_s T & \text{in } \Omega_s \\ \rho c_\ell T + \rho \bar{\ell} & \text{in } \Omega_\ell \end{cases} \quad (5)$$

and the latent heat is given by

$$\ell = (c_\ell - c_s)T_0 + \bar{\ell}. \quad (6)$$

Note that the variational principle (4) gathers all the equations of the Stefan model except for the interface condition (2b). The Stefan problem is thus to satisfy (4) and find the evolution of  $\Gamma(t)$  ensuring the condition (2b). The way to impose this condition will be detailed in section 3.

Integration by parts allows to rewrite (4) as

$$-\frac{d}{dt} \int_{\Omega(t)} \rho e(T) T^* \, d\Omega + \int_{\Omega(t)} k \nabla T \cdot \nabla T^* \, d\Omega + \int_{\Omega(t)} \rho e(T) \mathbf{w} \cdot \nabla T^* \, d\Omega = \int_{\Omega(t)} \rho S T^* \, d\Omega, \quad \forall T^* \in \mathcal{U}_0 \quad (7)$$

Using standard notations for scalar products in Hilbert spaces, equation (4) can be reformulated as where

$$\frac{d}{dt} (T(t), T^*)_t + a_t(T(t), T^*) + b_t(T(t), T^*, \mathbf{w}) = c_t(T^*), \quad \forall T^* \in \mathcal{U}_0 \quad (8)$$

where

$$(T, T^*)_t = \int_{\Omega(t)} \rho e(T) T^* \, d\Omega = \int_{\Omega(t)} \rho c T T^* \, d\Omega + \int_{\Omega(t)} \rho \bar{\ell} T^* \, d\Omega \quad (8a)$$

$$a_t(T, T^*) = \int_{\Omega(t)} k \nabla T \cdot \nabla T^* \, d\Omega \quad (8b)$$

$$b_t(T, T^*, \mathbf{w}) = \int_{\Omega(t)} \rho e(T) \mathbf{w} \cdot \nabla T^* \, d\Omega = \int_{\Omega(t)} \rho c T \mathbf{w} \cdot \nabla T^* \, d\Omega + \int_{\Omega(t)} \rho \bar{\ell} \mathbf{w} \cdot \nabla T^* \, d\Omega \quad (8c)$$

$$c_t(T^*) = \int_{\Omega(t)} \rho S T^* \, d\Omega \quad (8d)$$

## 2.2 Temperature update

The domain  $\Omega(t)$  is partitioned into a mesh  $\mathcal{M}$ , made of triangular elements  $e \in \mathcal{M}$  and nodes  $i \in \mathcal{N}$ , where  $\mathcal{N}$  is the set of the mesh nodes. In the X-MESH approach, the topology of the mesh, i.e. adjacencies between mesh entities will be kept fixed. Yet, positions of the nodes will be updated in an extreme fashion. In X-MESH, the front  $\Gamma(t)$  will be meshed at all times. In the context of the phase change problem, the front  $\Gamma$  is characterized by the condition  $T = T_0$  so this iso-temperature will explicitly appear as mesh edges of the triangular mesh. Vertex positions at time step  $t_n$  are thus noted  $\mathbf{X}^n$  and can be computed using extreme mesh deformations defined below in §3.

We use here a finite element semi-discretization in space variable  $\mathbf{x}$ :

$$T_h(\mathbf{x}, t) = \sum_{i \in \mathcal{N}} T_i(t) \phi_i(\mathbf{x}, t) \quad (9)$$

with  $\phi(\mathbf{x}, t)$  finite element basis of current configuration  $\Omega(t)$ . The Crank-Nicolson scheme to solve (8) writes:

$$\begin{aligned} & \left( [M^{n+1}] + \theta \Delta t [K^{n+1}] + \frac{\Delta t}{2} [L^{n+1/2}] \right) \mathbf{T}^{n+1} \\ &= \left( [M^n] - (1 - \theta) \Delta t [K^n] + \frac{\Delta t}{2} [L^{n+1/2}] \right) \mathbf{T}^n + [P^n] - [P^{n+1}] + \Delta t \left( [S^{n+1/2}] - [Q^{n+1/2}] \right) \end{aligned} \quad (10)$$

where

$$M_{ij}^n = \int_{\Omega(t_n)} \phi_i(\mathbf{x}, t_n) \rho c(\mathbf{x}, t_n) \phi_j(\mathbf{x}, t_n) \, d\Omega \quad (11a)$$

$$K_{ij}^n = \int_{\Omega(t_n)} \nabla \phi_i(\mathbf{x}, t_n) k(\mathbf{x}, t_n) \nabla \phi_j(\mathbf{x}, t_n) \, d\Omega \quad (11b)$$

$$L_{ij}^n = \int_{\Omega(t_n)} \nabla \phi_i(\mathbf{x}, t_n) \rho c(\mathbf{x}, t_n) \mathbf{w}^n \phi_j(\mathbf{x}, t_n) \, d\Omega \quad (11c)$$

$$P_i^n = \int_{\Omega_\ell(t_n)} \phi_i(\mathbf{x}, t_n) \rho \bar{\ell}(\mathbf{x}, t_n) \, d\Omega \quad (11d)$$

$$Q_i^n = \int_{\Omega_\ell(t_n)} \nabla \phi_i(\mathbf{x}, t_n) \rho \cdot \bar{\ell}(\mathbf{x}, t_n) \mathbf{w}^n \, d\Omega \quad (11e)$$

$$S_i^n = \int_{\Omega(t_n)} \rho S \phi_i(\mathbf{x}, t_n) \, d\Omega \quad (11f)$$

Note that (10) uses some predicted quantities at time  $t_{n+1/2}$  defined on  $\Omega(t_{n+1/2})$ , which require the predicted mesh nodes positions  $\mathbf{X}^{n+1/2}$ . It is defined as

$$\mathbf{X}^{n+1/2} = \frac{\mathbf{X}^n + \mathbf{X}^{n+1}}{2} \quad (12)$$

The corresponding predicted mesh nodes speed is

$$\mathbf{w}^{n+1/2} = \frac{\mathbf{X}^{n+1} - \mathbf{X}^n}{\Delta t} \quad (13)$$

And we define  $\bar{\ell}^{n+1/2}$  as

$$\bar{\ell}^{n+1/2} = \frac{\bar{\ell}^n + \bar{\ell}^{n+1}}{2} \quad (14)$$

Note here that  $\Omega(t_n)$  actually depends on  $\mathbf{T}^n$  so the problem (10) is non-linear.

### 3 Front relaying

The X-MESH approach consists in always having the front  $\Gamma$  that belongs to the mesh. Figure 3 illustrates the strategy used to locally move the nodes of a two-dimensional triangular mesh to track a moving front defined by a level-set function. First the active nodes are tagged (b). A node is considered active if it was on the front at the end of the previous iteration (a) or if the sign of its level-set value has changed compared to the previous iteration (b vs a). Next, the possible targets of each active nodes are listed (c). Target points are the location of the zeros of the level-set field interpolated along an edge connecting the active node to an inactive node. Edges connecting two active nodes are excluded. Then, the active nodes are moved to the position of their nearest target (boundary nodes are only allowed to move along their boundaries) and compose the new front nodes (d). Active nodes without target are removed from the front. Finally, the positions of all nodes, except the front nodes, are relaxed toward their positions in the original mesh.

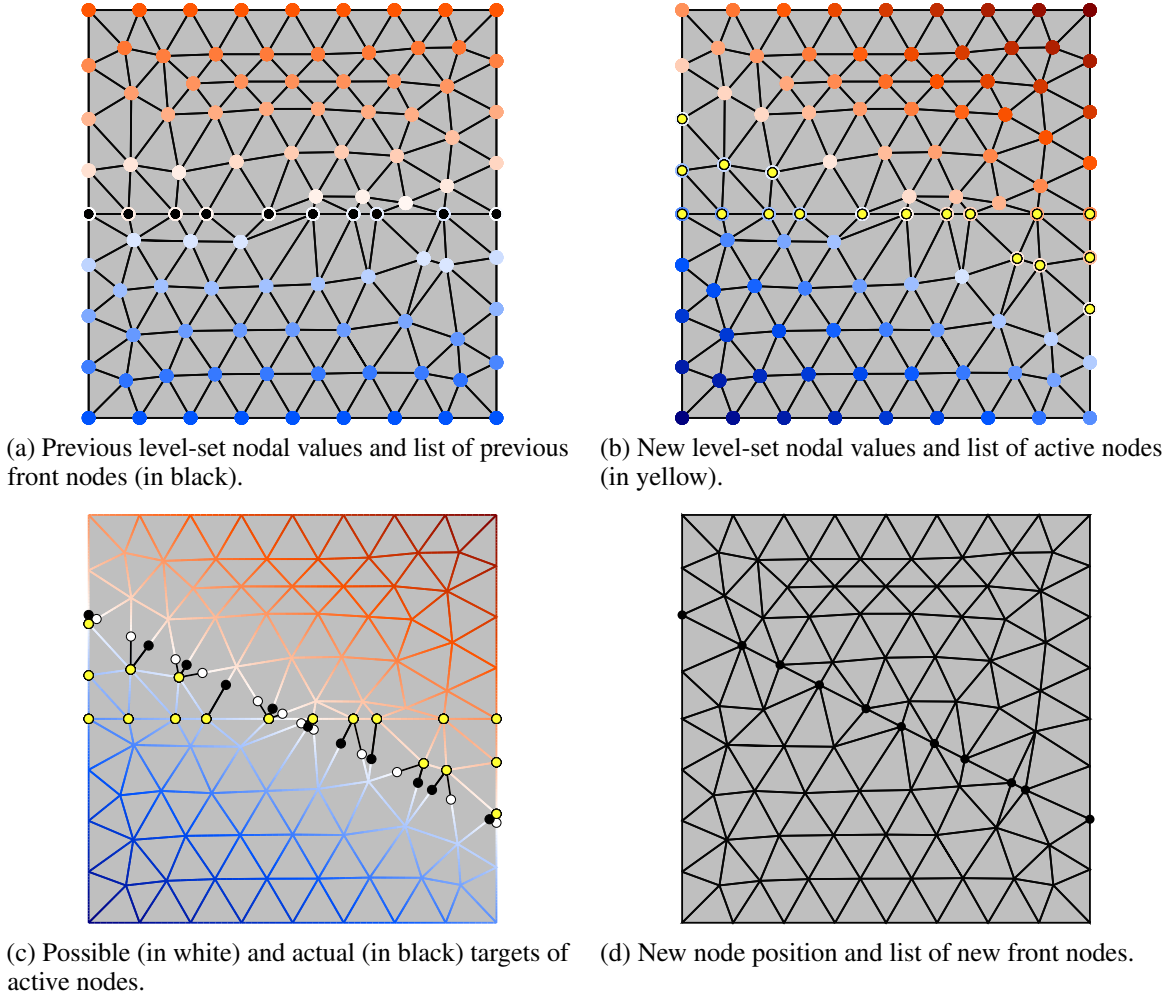


Figure 3: Front-relaying local adaptation of a triangular mesh to track a front defined by a level-set.

This procedure – called *surface relaying* – although quite simple introduces the possibility of reducing the element sizes to zero. Figure 4 how front relaying is able to track a moving levelset that has the shape of a growing circle. Timesteps that are used in this artificial example are very small, way smaller than the ones that are chosen in usual Stefan problem computations but it allows to visualize the emergence of zero- or quasi-zero measure elements. In Babuska and Aziz [1976], authors prove that a sufficient condition for having convergent finite element solution when the mesh is refined is that angles should be bounded from above and thus forbid zero- or obtuse nearly zero-measure elements. Mesh algorithms are thus supposed to try their best to generate *quality meshes* in that sense Shewchuk [2002]. This conclusion has been mitigated since. In Hannukainen et al. [2012a], it is shown that there exist meshes that do not respect the angle condition and that converge anyway. Some authors have also wisely noted that the angle condition is only a sufficient condition Hannukainen et al. [2012b] and that this condition can be largely weakened Kučera [2016]. In reality, it has been proven that optimally convergent finite element solutions can be obtained with meshes that are *visually unpleasant*. The family of computationally acceptable meshes can thus include patterns of badly shaped elements Duprez et al. [2019] like isolated caps (a cap is a very obtuse triangles) but also can consist in more complex structures as bands or clusters. In his paper Kučera [2016], Pr. Kučera claims that “one can fabricate very strange triangulations satisfying the assumptions of the theory presented. Such meshes perhaps do not have any value from the practical point of view”. In our perspective, these “wild” meshes are indeed very useful from the practical point of view and are at the core of what is proposed here.

Visually unpleasant, yet acceptable patterns in a mesh only harms the conditioning of the finite element matrices Duprez et al. [2019]. In this paper, we will deform meshes in such a way that they always conform to a moving interface using

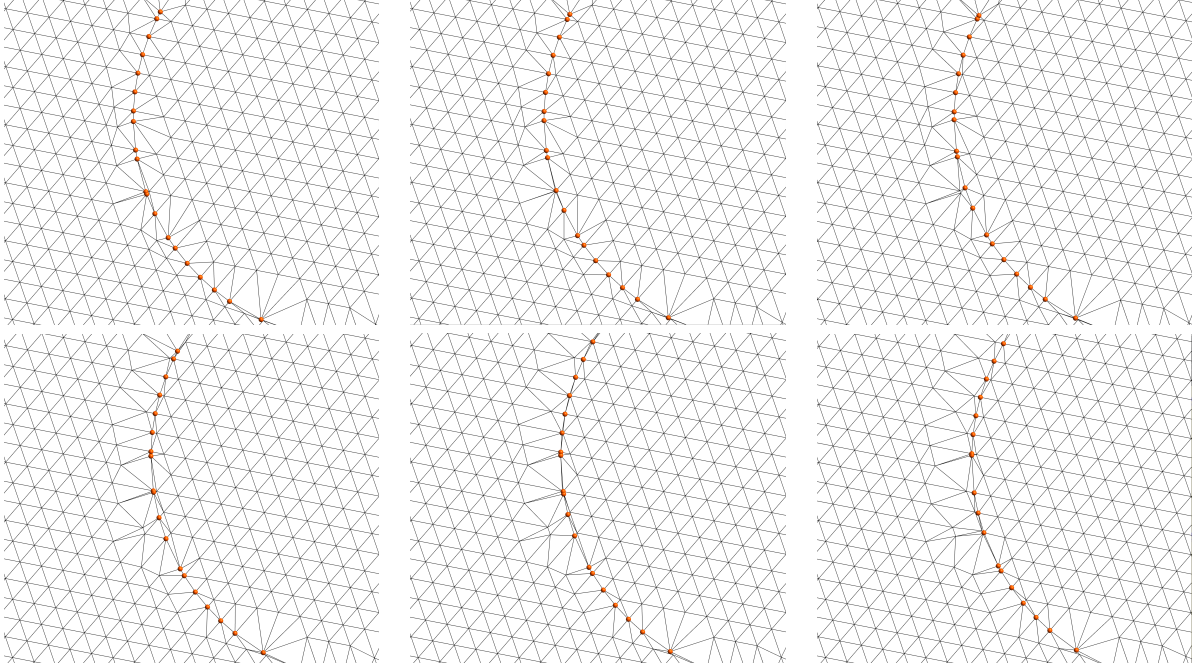


Figure 4: Front relaying in dimension 2

relaying. Fronts will be seeded and anihilated as well and all that using a mesh with the same adjacencies i.e. the same number of nodes and the adjacencies between mesh entities.

#### 4 Staggered scheme

In this paper we will consider a staggered algorithm, summarized in algorithm 1. In what follows,  $n$  will denote the current time step and  $k$  the current iteration. At each time step  $n$ , a first value of the new nodal temperature vector  $\mathbf{T}_0^{n+1}$  is computed for a fixed mesh. Then, using this temperature field, the mesh is updated while keeping the temperature fixed, which gives a new position of the mesh nodes  $\mathbf{X}_0^{n+1}$ . This new position of the mesh is used to compute the new temperature field  $\mathbf{T}_1^{n+1}$ , and so on. The procedure is iterated  $k$  time until the  $L_2$ -norm of the increment over one iteration falls bellow a prescribed tolerance:

$$\text{err}^2 = \int_{\Omega} (T_k^{n+1} - T_{k-1}^{n+1})^2 \, d\Omega < \text{tol}^2 \quad (15)$$

To solve numerically the Stephan problem, we need to determine, for each time step  $n$ :

- The vector of nodal temperature  $\mathbf{T}^n$  (nodal quantity)
- The position of the mesh nodes  $\mathbf{X}^n$  (nodal quantity)

From these two quantities, we can obtain:

- The mesh nodes velocity vector  $\mathbf{w}^n$  (nodal quantity)
- The phase vector  $\phi^n$  (element-wise quantity), for which each component  $\phi_e^n$  indicates if element  $e$  at time step  $n$  is in the liquid or the solid phase
- The material properties vectors  $\mathbf{c}^n, \mathbf{k}^n, \bar{\ell}^n$  (element-wise quantity) which contains the material properties on each element at time  $n$

Note that for a given couple  $(T^n, X^n)$ , the quantities  $\phi^n, c^n, k^n, \bar{\ell}^n$  can be easily determined by looking at the sign of  $T_i^n - T_0$  at each node  $i$ , a process that we note

$$(\phi^n, c^n, k^n, \bar{\ell}^n) = \text{UPDATE}(T^n, X^n) \quad (16)$$

For a given element  $e$ , if all the nodal values of  $T^n$  are greater than  $T_0$ , then  $\phi_e = \ell$ ,  $c_e = c_\ell$ ,  $k_e = k_\ell$ ,  $\bar{\ell}_e = \bar{\ell}$ . Otherwise, if all the nodal values of  $T^n$  are smaller than  $T_0$ , then  $\phi_e = s$ ,  $c_e = c_s$ ,  $k_e = k_s$ ,  $\bar{\ell}_e = 0$ .

---

**Algorithm 1:** Staggered resolution

---

```

1 Initialization ;
2 Set  $n = 0$  ;
3 Initialize  $T^0, X^0$  ;
4 Initialize  $\phi^0, c^0, k^0, \bar{\ell}^0$  ;
5 while  $n < n_{\max}$  do
6   Initialize ;
7    $k = 0$  ;
8    $X_0^{n+1} = X^n$  ;
9    $w_0^{n+1} = 0$  ;
10  Initialize material properties:  $(\phi_0^{n+1}, c_0^{n+1}, k_0^{n+1}, \bar{\ell}_0^{n+1}) = \text{UPDATE}(T^n, X^n)$  ;
11  while  $k < k_{\max}$  do
12    Compute predicted mesh position  $X_k^{n+1/2}$  using (12) with  $X^n$  and  $X_k^{n+1}$  ;
13    Compute predicted mesh nodes speed  $w_k^{n+1/2}$  using (13) with  $w_k^n$  and  $w_k^{n+1}$  ;
14    Compute prediction  $\bar{\ell}_k^{n+1/2}$  using (14) with  $\bar{\ell}^n$  and  $\bar{\ell}_k^{n+1}$  ;
15    Solve (10) to find  $T_{k+1}^{n+1}$ , replacing  $(\bullet)^{n+1}$  by  $(\bullet)_k^{n+1}$  and  $(\bullet)^{n+1/2}$  by  $(\bullet)_k^{n+1/2}$  ;
16    Move nodes on iso zero of  $T_{k+1}^{n+1}$  to obtain  $X_{k+1}^{n+1}$  (see section 3) ;
17    Update material properties:  $(\phi_{k+1}^{n+1}, c_{k+1}^{n+1}, k_{k+1}^{n+1}, \bar{\ell}_{k+1}^{n+1}) = \text{UPDATE}(T_{k+1}^{n+1}, X_{k+1}^{n+1})$  ;
18    Compute err (see equation (15));
19    if  $err < tol$  then
20      go to 5 ;

```

---

## 5 A basic more evolved scheme: semi-monolithic scheme

The temperature update to compute  $T^{n+1}$  detailed in section 2.2 is a linear problem, which is solved for a fixed mesh configuration. It has been observed that for a value of the latent heat  $\ell = 0$ , the convergence of the staggered scheme is pretty good, however for  $\ell > 0$  it is not the case anymore; the higher  $\ell$ , the higher the number of iterations to reach convergence is, and in the worse case it may not converge at all. We believe that the higher  $\ell$ , the stronger is the coupling between  $T$  and the mesh nodes configuration.

The best way to solve the problem would be to write a proper Newton-Raphson resolution which would take into account the variation of the temperature field with the mesh nodes displacement. However, since the full linearization would be complex to write, we tried to implement a pseudo Newton resolution, where we still update the temperature for a fixed mesh, but considering that  $w$  depends on temperature.

The residual is computed for each node  $i \in \mathcal{N}$  as:

$$\begin{aligned}
f_i = & \int_{\Omega} ((\rho c)^{n+1} T^{n+1} + (\rho \bar{\ell})^{n+1}) T_i^{*n+1} d\Omega - \int_{\Omega} ((\rho c)^n T^n + (\rho \bar{\ell})^n) T_i^{*n} d\Omega \\
& + \theta \Delta t \int_{\Omega} k^{n+1} \nabla T^{n+1} \cdot \nabla T_i^{*n+1} d\Omega + (1 - \theta) \Delta t \int_{\Omega} k^n \nabla T^n \cdot \nabla T_i^{*n} d\Omega \\
& + \frac{\Delta t}{2} \int_{\Omega} ((\rho c)^{n+1} T^{n+1} + (\rho \bar{\ell})^{n+1}) \mathbf{w} \cdot \nabla T_i^{*n+\frac{1}{2}} d\Omega + \frac{\Delta t}{2} \int_{\Omega} ((\rho c)^n T^n + (\rho \bar{\ell})^n) \mathbf{w} \cdot \nabla T_i^{*n+\frac{1}{2}} d\Omega
\end{aligned} \quad (17)$$

where  $\mathbf{w} = \frac{X^{n+1} - X^n}{\Delta t}$  is the mesh nodes velocity. We search  $T^{n+1}$  such that:

$$f_i(T^{n+1}, T^n, \Omega_f^{n+1}, \Omega_f^n, \Omega_s^{n+1}, \Omega_s^n, \mathbf{w}) = 0 \quad \forall i \in \mathcal{N} \quad (18)$$

Properties	Units	Symbol	Solid	Liquid	Interface
Volumic mass	kg.m <sup>-3</sup>	$\rho$	1000	1000	
Specific heat capacity	J.K <sup>-1</sup> .kg <sup>-1</sup>	$c$	2090	4185	
Conductivity	W.m <sup>-1</sup> .K <sup>-1</sup>	$k$	2.1	0.6	
Latent heat	J.K <sup>-1</sup>	$\ell$			0 / 330000
Phase change temperature	K	$T_0$			273

Table 1: Material properties of 1D Stefan test case

where  $\Omega_f^{n+1}$ ,  $\Omega_s^{n+1}$  and  $\mathbf{w}$  are functions of the nodal values of  $T^{n+1}$ .

A regular newton iteration  $k$  reads:

$$T^{n+1,k+1} = T^{n+1,k} - r^{n+1,k} \quad (19)$$

$$\mathbf{X}^{n+1,k+1} = \text{move front}(\mathbf{X}^{n+1,k}, T^{n+1,k}, T^{n+1,k+1}) \quad (20)$$

where “move front” was explained in 3, and  $r^{n+1,k}$  is the solution of the linear system (from now on, the  $k$  indices are omitted)

$$Ar^{n+1} = f_i(T^{n+1}) \quad (21)$$

Unfortunately, we are not able to evaluate

$$A_{ij} = \frac{df_i}{dT_j^{n+1}} \quad (22)$$

and we switch to a quasi-Newton method by substituting  $A_{ij}$  with:

$$B_{ij} = \frac{\partial f_i}{\partial T_j^{n+1}} + C_{ij} \quad (23)$$

The first part of  $B$  is the linearization of  $f$ , ignoring the dependency in  $T^{n+1}$  of  $\mathbf{X}^{n+1}$ ,  $c^{n+1}$ ,  $k^{n+1}$  and  $\bar{l}^{n+1}$ .

$$\frac{\partial f_i}{\partial T_j^{n+1}} = \int_{\Omega} (\rho c)^{n+1} T_j^{*n+1} T_i^{*n+1} d\Omega \quad (24)$$

$$+ \theta \Delta t \int_{\Omega} k^{n+1} \nabla T_j^{*n+1} \cdot \nabla T_i^{*n+1} d\Omega \quad (25)$$

$$+ \frac{\Delta t}{2} \int_{\Omega} (\rho c)^{n+1} T_j^{*n+1} \mathbf{w} \cdot \nabla T_i^{*n+\frac{1}{2}} d\Omega \quad (26)$$

And  $C_{ij}^k$  is an incomplete and probably incorrect attempt to partially take the front displacement into account in the linearization:

$$C_{ij}^k = -\Delta t \int_{\Gamma^{n+1}} \rho \bar{l} \frac{d\mathbf{w}}{dT_j^{n+1,k}} \cdot \mathbf{n} T_i^{*n+1} d\Gamma \quad (27)$$

To summarize, the semi-monolithic algorithm is exactly the same as the staggered algorithm explained in algorithm 1, except that the computation of  $T_{k+1}^{n+1}$  is done by equation (19) instead of equation (10). Although this linearization is partial, we will see 6 that it allows to get some interesting results.

## 6 Numerical examples

The X-MESH approach is tested on several examples. The numerical values of the thermal properties, unless noted otherwise, are given in table 1. A summary of the different test cases with the resolution method used (staggered/semi-monolithic scheme) is given in table 2.

### 6.1 The straight front semi-infinite two phase problem ( $\ell = 0$ )

The straight front two-phase Stefan problem can be expressed as a heat conduction problem in a semi-finite domain represented by  $\Omega = [0, +\infty]$ . There is no volumic heat source. The domain is initially liquid at temperature  $T_\ell = 293\text{K}$  and the temperature is abruptly lowered at the temperature  $T_s = 263\text{K}$  at the left side of the slab. A solidification front



Problem	Resolution	Value of $\ell$ (J.K <sup>-1</sup> )	Description	Section
Straight front semi-infinite	Staggered	0	Analytical boundary condition	6.1
Axisymmetric	Staggered	0	Analytical boundary condition	6.2
Mutliple melting fronts	Staggered	0	Initial temperature field	6.3
Mutliple heat sources	Staggered	0	Multiple heat sources	6.4
Moving heat source	Staggered	0	Moving heat source + Boundary temperature	6.5
Straight front semi-infinite	Semi-monolithic	330 000	Analytical boundary condition	6.6

Table 2: Numerical examples summary

represented by  $x_f(t)$  is created an moves continuously in the right direction. It is given (see Carslaw and Jaeger [1959]) by

$$x_f(t) = 2\phi\sqrt{\beta_s t} \quad (28)$$

where  $\beta_s = \frac{k_s}{\rho c_s}$  and  $\phi$  is a numerical parameter obtained by solving

$$\frac{e^{-\phi^2}}{\text{erf}(\phi)} - \frac{k_\ell}{k_s} \frac{\sqrt{\eta}(T_\ell - T_0)e^{-\eta\phi^2}}{(T_0 - T_s)(1 - \text{erf}(\phi\sqrt{\eta}))} - \frac{\phi L\sqrt{\pi}}{\rho c_s(T_0 - T_s)} = 0 \quad (29)$$

where  $\beta_\ell = \frac{k_\ell}{\rho c_\ell}$  and  $\eta = \beta_s/\beta_\ell$

The configuration of the problem is thus varying in time. We have  $\Omega(t) = \Omega_\ell(t) \cup \Omega_s(t)$  with  $\Omega_s(t) = [0, x_f]$  and  $\Omega_\ell(t) = [x_f, +\infty]$ . The temperature field in the solid phase is given by

$$T(x) = T_s + \frac{(T_0 - T_s)}{\text{erf}(\phi)} \text{erf}\left(\frac{x}{2\sqrt{\beta_s t}}\right), \text{ for } x \in \Omega_s \quad (30)$$

and in the liquid phase by

$$T(x) = T_\ell - \frac{(T_\ell - T_0)}{(1 - \text{erf}(\phi\sqrt{\eta}))} \left(1 - \text{erf}\left(\frac{x}{2\sqrt{\beta_\ell t}}\right)\right), \text{ for } x \in \Omega_\ell \quad (31)$$

Although the geometry of the problem is 1D and semi-infinite, we use a square domain of dimension  $0.1 \times 0.1$  m, imposing the exact solution on the right boundary to simulate the infite boundary condition. Computations are performed with  $\ell = 0$ , using the staggered scheme (see 4). The domain is meshed with order 1 triangular elements with a characteristic size of  $h_e$ . To avoid the singularity at  $t = 0$ , the simulation starts at  $t_0 = 900$  s, with a time step of  $\Delta t 50 h_e \sqrt{t}$ . The results obtained for  $h_e = 0.01$  m are presented on figure 5. The numerical front position is computed by taking the average  $x$  coordinates of the phase change front nodes. One can observed that the front nodes are perfectly aligned on a vertical straight line. On figure 6 are presented the results for different values of  $h_e$ . Whatever the value of  $\ell$ , the front is correctly captured; the relative error with respect to the the analytical solution is less than 1%, even with the coarsest mesh. The results show a good converge with mesh refinement.

## 6.2 The axisymmetric two phase problem

The next example is the axisymmetric problem of the solidification of a liquid domain due to a heat sink  $Q$  located at  $r = 0$ . At  $t = 0$ , the temperature is uniform, equal to  $T_i$ . Then, for any time  $t \in [0, T_{\max}]$ , the position of the solidification front (see Carslaw and Jaeger [1959]) is given by

$$r_f(t) = 2\phi\sqrt{\beta_s t} \quad (32)$$

where the numerical parameter  $\phi$  is obtained by solving

$$\frac{Q}{4\pi} e^{-\phi^2} + \frac{k_\ell(T_i - T_0)}{Ei(-\phi^2\eta)} \exp(-\phi^2\eta) - \phi^2 \rho \beta_s L = 0 \quad (33)$$

The temperature in the solid phase is given by

$$T(r) = T_0 + \frac{Q}{4\pi k_s} \left[ Ei\left(-\frac{r^2}{4\beta_s t}\right) - Ei(-\phi^2) \right], \text{ for } x \leq r_f \quad (34)$$

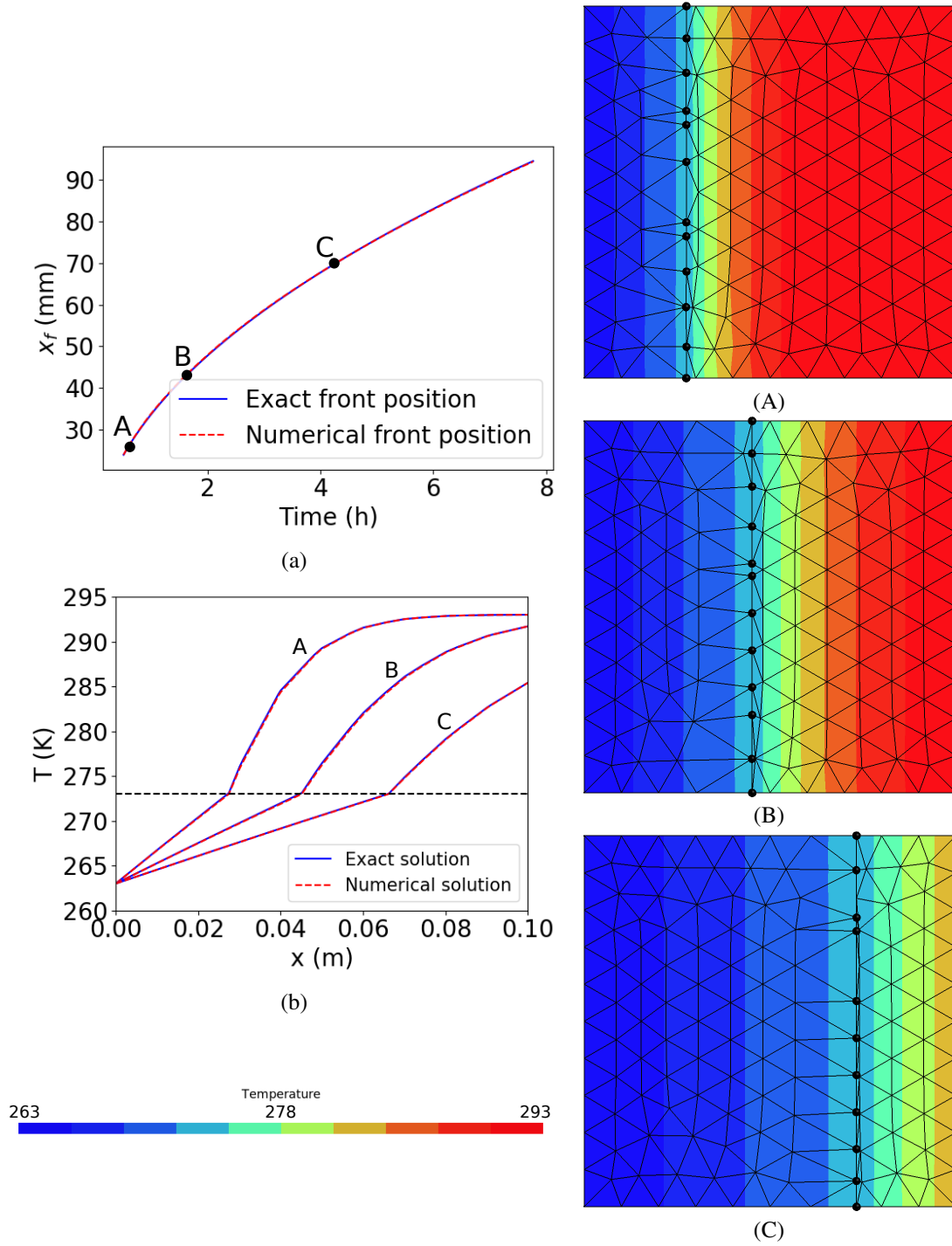


Figure 5: Stefan straight front problem: numerical results for  $\ell = 0$  and  $h_e = 0.01$  m. a. Comparison of exact and numerical front position. b. Analytical and numerical solutions (left) and corresponding temperature fields and fronts (right) at  $t = 0.66$  h (A),  $1.78$  h (B) and  $t = 4.68$  h (C)

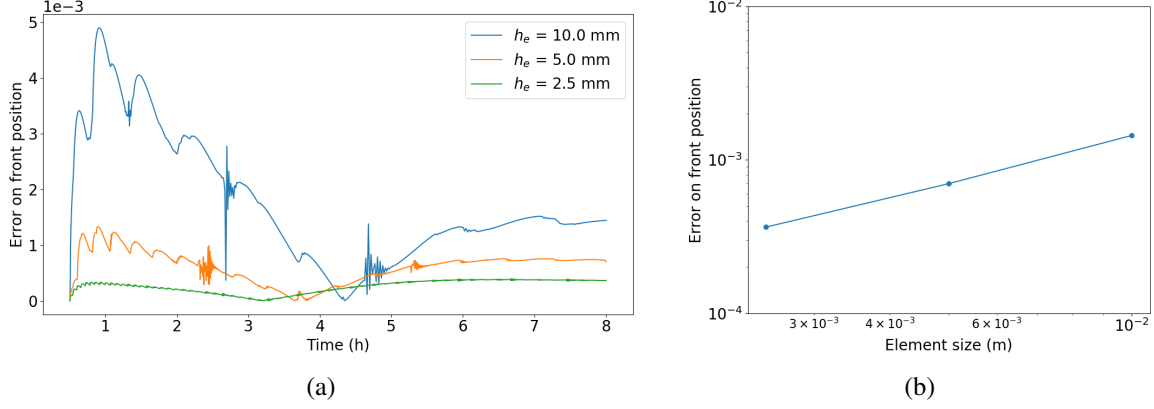


Figure 6: Stephan straight front problem: error comparisons for  $\ell = 0$ . a. Comparison of error for different mesh element sizes. b. Convergence with mesh refinement

and the temperature in the liquid phase by

$$T(\mathbf{x}) = T_i - \frac{T_i - T_0}{Ei(-\phi^2\eta)} Ei\left(-\frac{r^2}{4\beta_\ell t}\right), \text{ for } x \geq r_f \quad (35)$$

Computations are performed with  $\ell = 0$ , using the staggered scheme (see 4). The initial temperature is  $T_i = 293$  K and the heat sing strength  $Q = 100 \text{ J.m}^{-3}$ . To take into account both the singularity of the solution at  $r = 0$  and the infinite boundary condition, the simulated domain is a ring with interior radius  $R_{\text{int}} = 0.01$  m and exterior radius  $R_{\text{ext}} = 0.1$  m, where the analytical temperature is applied as boundary condition. The time step is  $\Delta t = 1000h_e\sqrt{t}$ . The results obtained for a coarse mesh with a finite element size  $h_e = 0.005$  m are given in figure 7, and the error for different mesh element size is plotted in figure 8. For the former one, the numerical value of the front position which is plotted and used to compute the error is obtained by taking the average of the  $r$  coordinate of the nodes of the phase-change front. Here again, the front is correctly captured by the X-MESH approach. Contrary to the previous test case, the error is always decreasing with mesh element size (see figure 8 (a)).

### 6.3 Multiple melting fronts problem

In this example we simulate the evolution of an initial temperature field on a square domain of dimensions  $3 \times 3$  m, without any boundary conditions or heat source. The problem is solved with the staggered algorithm and  $\ell = 0$ . The time step is  $\Delta t = 1000$  s. The initial temperature field (see figure 9 (A)) has above  $T_0$  and below  $T_0$  zones, with multiple fronts. The solid zones progressively melt until there is only liquid. This example illustrate the capacity of the X-MESH method to annihilate fronts.

### 6.4 Multiple heat sources problem

In this example we start from an initial uniform temperature field  $T_i = 263$  K below freezing temperature, on a square domain of dimensions  $3 \times 3$  m. As illustrated on figure 10, three heat sources are applied near the center of the domain. The problem is solved with the staggered algorithm and  $\ell = 0$ . The time step is  $\Delta t = 1000$  s. Initially, there is no front. Then, due to the heat sources, the temperature grows above  $T_0$ , and phase-change fronts start to nucleate (figure 10 (B)). The liquid zones grow, until merging with each other (figure 10 (E)). This example illustrate the capacity of the X-MESH method to seed new fronts, as well as the capacity to merge existing fronts between each other.

### 6.5 Moving heat source problem

Figure 11 shows different snapshots of a phase change problem that actually mimics the motion of a heat source following a  $\infty$  path. The algorithm is perfectly stable with about 5 staggered iterations to converge the position of the front.

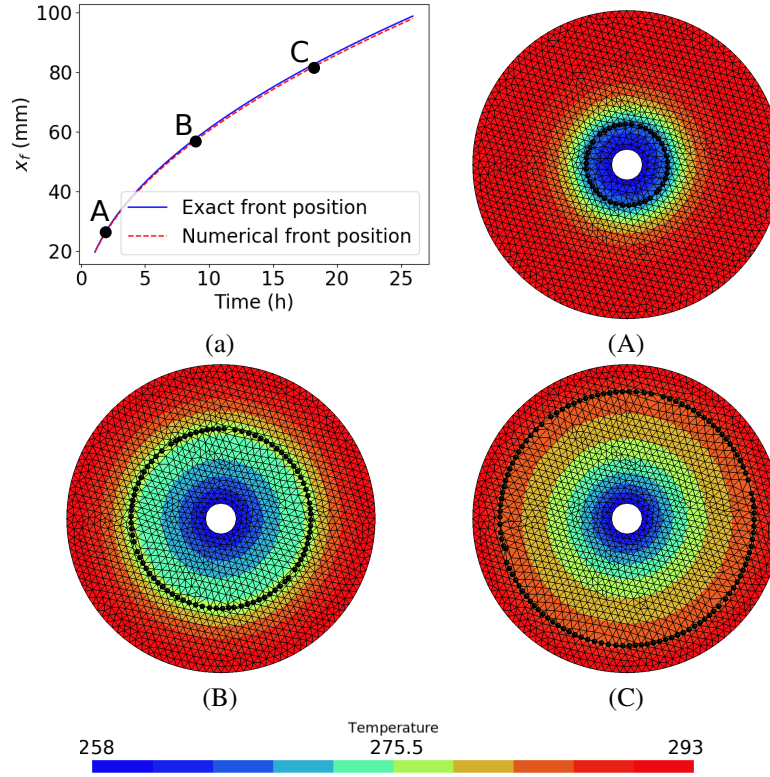


Figure 7: Stefan axisymmetric problem: numerical results for  $\ell = 0$  for  $h_e = 0.005$  m. a. Comparison of exact and numerical front position. Temperature fields and fronts at  $t = 2.1$  h (A),  $9.6$  h (B) and  $t = 18.9$  h (C)

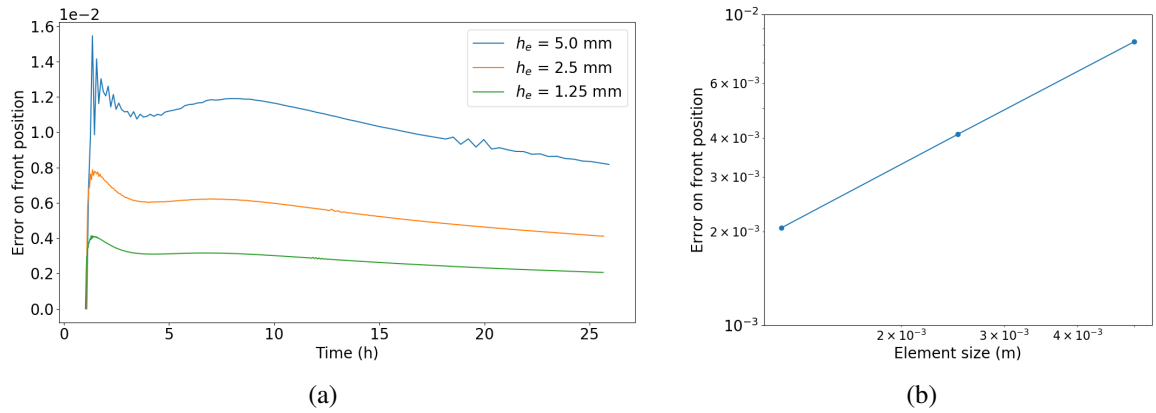


Figure 8: Stefan axisymmetric problem: error comparisons for  $\ell = 0$ . a. Comparison of error for different mesh element sizes. b. Convergence with mesh refinement

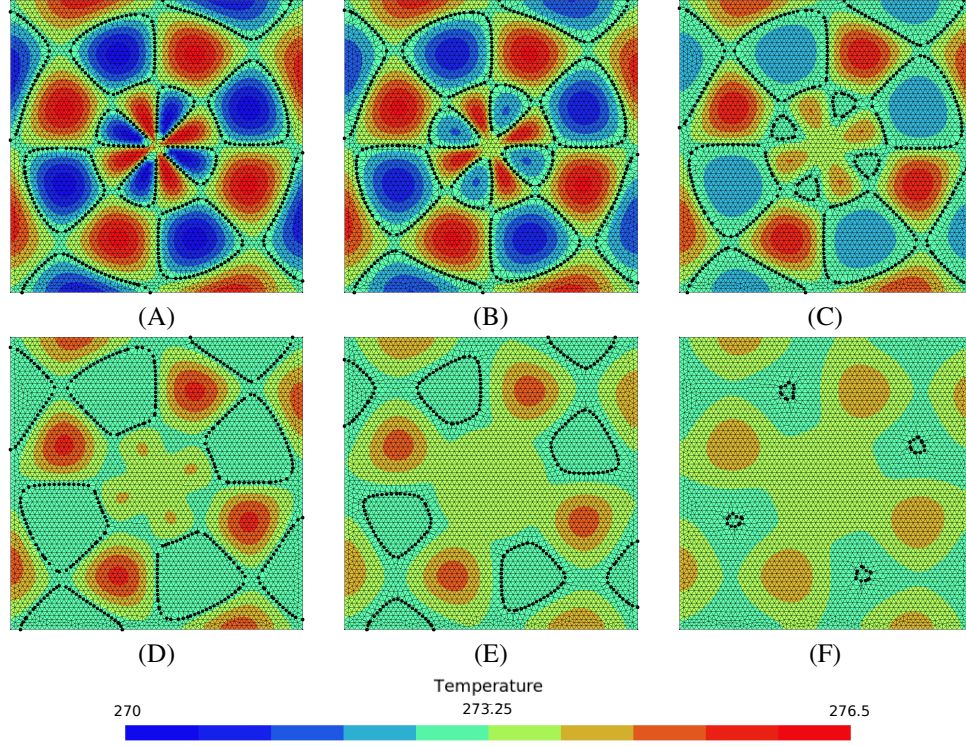


Figure 9: Stephan multiple melting fronts problem, temperature fields at (A)  $t = 0$  h (B)  $t = 1.66$  h (C)  $t = 8.33$  h (D)  $t = 16.66$  h (E)  $t = 30.55$  h (F)  $t = 44.44$  h

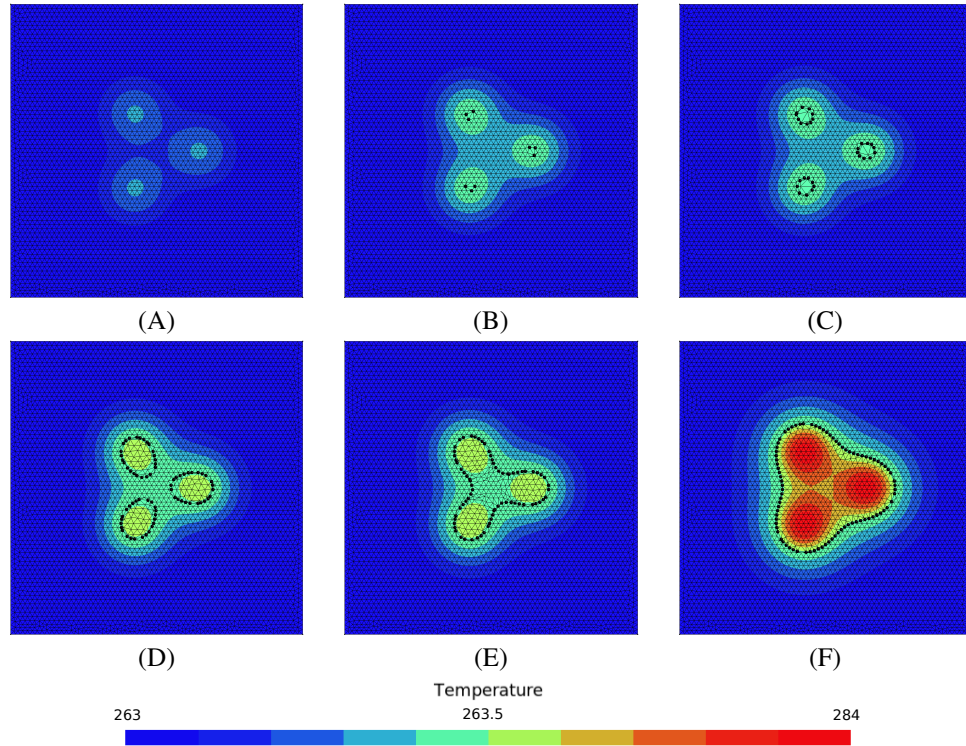


Figure 10: Stephan multiple heat sources problem, temperature fields at (A)  $t = 5.55$  h (B)  $t = 9.44$  h (C)  $t = 10$  h (D)  $t = 12.5$  h (E)  $t = 13$  h (F)  $t = 26.39$  h



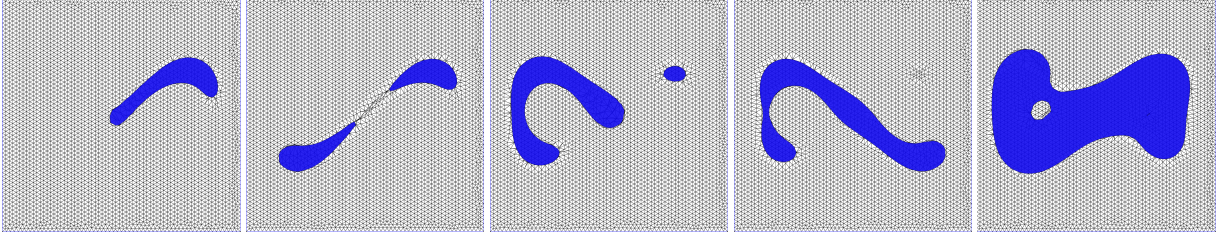


Figure 11: Phase change problem using Stefan model (liquid phase is in blue). One hot spot is moving on a  $\infty$  shape path, creating solid  $\rightarrow$  liquid phase change. The boundary of the domain is maintained at temperature that corresponds to a solid phase. 165 time steps were required to go from the left to the right image. This simulation has been done on a fixed topology mesh with extreme deformations that include seeding, relaying and annihilation.

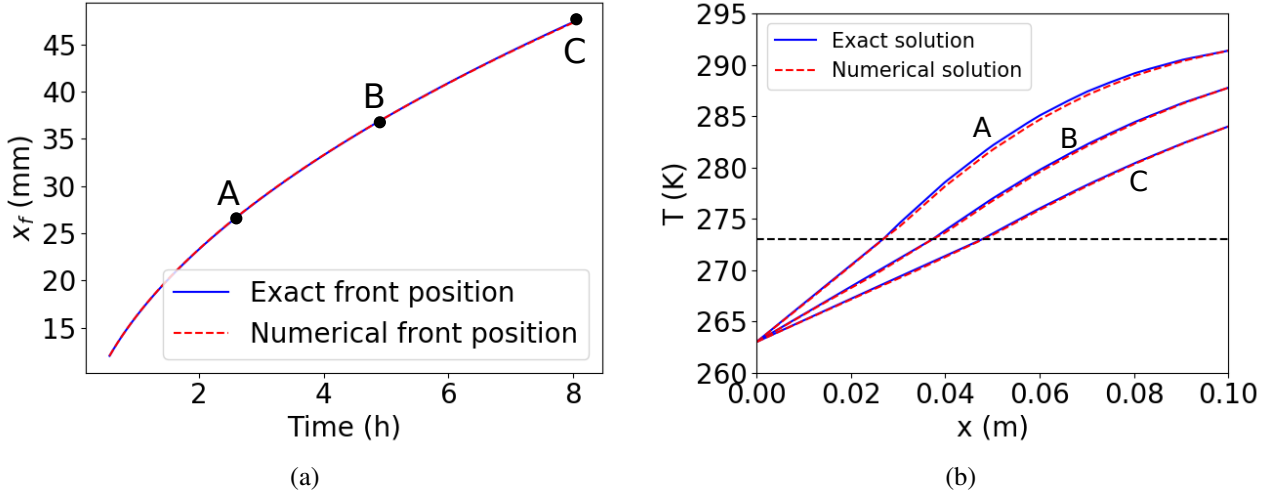


Figure 12: Stefan straight front problem: numerical results for  $\ell = 330000 \text{ J.K}^{-1}$  and  $h_e = 0.01 \text{ m}$ . a. Comparison of exact and numerical front position. b. Comparison of exact and numerical temperature field along  $x$  for  $t = 2.62 \text{ h}$  (A),  $t = 5 \text{ h}$  (B), and  $t = 8 \text{ h}$  (C).

### 6.6 The straight front semi-infinite two phase problem ( $\ell > 0$ )

In this section, the same problem as in section 6.1 is solved, but with a latent heat  $\ell = 333000 \text{ J.K}^{-1}$  and the semi-monolithic scheme of section 5. The time step is  $\Delta t = 50 h_e \sqrt{t}$ . The results obtained for  $h_e = 0.01 \text{ m}$  are presented on figure 12. On figure 13 are presented the results for different values of  $h_e$ . Whatever the mesh element size, the relative error with respect to the analytical solution is less than 1%, however the convergence is not as good as in section 6.1. Also, the number of iterations necessary to reach convergence at each time step is about one order of magnitude bigger with a non-null latent heat. This is not surprising, considering the fact that the linearization proposed is 5 is partial; however, considering the low level of errors obtained, it can be considered as a good first and relatively easy to implement solution. Note that with the staggered scheme, and in view of the high value of  $\ell$ , the results would not even converge.

## 7 Conclusion

In this paper, a new method to address the Stefan problem has been introduced. The extreme mesh deformation approach (X-MESH) tracks the solidification/melting front without remeshing and with a classical finite element formulation. Moreover, the topology of the mesh is kept fixed. The X-MESH introduces the notion of front relaying allowing to keep an optimal mesh quality, at least for elements which are not directly connected to the front. The elements in contact with the front may have zero size during the computation. To deal with these zero- or close to zero-measure element, we have used an added volume approach but we plan to replace it with dualization which will not require any volume approximation. In this paper, we proposed a staggered resolution algorithm, where the temperature field is first computed for a given mesh configuration, then the mesh nodes are moved on the phase-change front. This

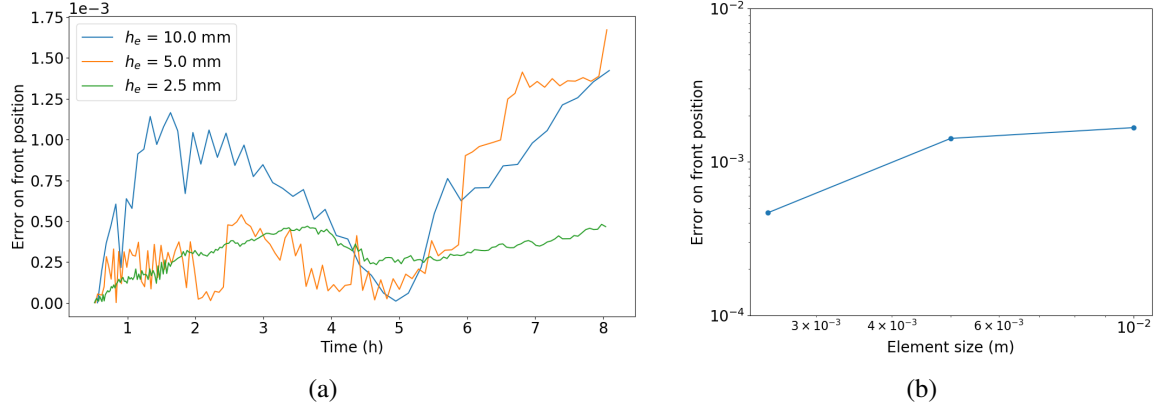


Figure 13: Stephan straight front problem: error comparisons for  $\ell = 330000 \text{ J.K}^{-1}$ . a. Comparison of error for different mesh element sizes. b. Convergence with mesh refinement

algorithm gives good results for zero latent heat, however for non null latent heat it may not converge, because of the stronger coupling between the temperature variation and the mesh nodes movements. A first, partial, attempt to account for this coupling was proposed in a semi-monolithic scheme. The results obtained with this approximation are quite good. We illustrated on examples with complex front geometries that the X-MESH approach allows to accurately represent sharp interfaces movements even in the case of topological changes.

## References

- M.A. Jaafar, D.R. Rousse, S. Gibout, and J.-P. Bédécarrats. A review of dendritic growth during solidification: Mathematical modeling and numerical simulations. 2017. doi:10.1016/j.rser.2017.02.050. URL <http://dx.doi.org/10.1016/j.rser.2017.02.050>.
- M. J. Baines, M. E. Hubbard, P. K. Jimack, and R. Mahmood. A moving-mesh finite element method and its application to the numerical solution of phase-change problems. *Communications in Computational Physics*, 6(3):595–624, 2009. ISSN 18152406. doi:10.4208/cicp.2009.v6.595.
- E. Gros, G. Anjos, and J. Thome. Moving mesh method for direct numerical simulation of two-phase flow with phase change. *Applied Mathematics and Computation*, 339:636–650, 2018. ISSN 0096-3003. doi:<https://doi.org/10.1016/j.amc.2018.07.052>. URL <https://www.sciencedirect.com/science/article/pii/S0096300318306180>.
- Yu Zhang, Anirban Chandra, Fan Yang, Ehsan Shams, Onkar Sahni, Mark Shephard, and Assad A. Oberai. A locally discontinuous ALE finite element formulation for compressible phase change problems. *Journal of Computational Physics*, 393:438–464, 2019. ISSN 10902716. doi:10.1016/j.jcp.2019.04.039. URL <https://doi.org/10.1016/j.jcp.2019.04.039>.
- S. Chen, B. Merriman, S. Osher, and P. Smereka. A Simple Level Set Method for Solving Stefan Problems. *Journal of Computational Physics*, 135(1):8–29, 1997. ISSN 00219991. doi:10.1006/jcph.1997.5721.
- Javed Shaikh, Atul Sharma, and Rajneesh Bhardwaj. On sharp-interface level-set method for heat and/or mass transfer induced Stefan problem. *International Journal of Heat and Mass Transfer*, 96:458–473, 2016. ISSN 00179310. doi:10.1016/j.ijheatmasstransfer.2015.12.074. URL <http://dx.doi.org/10.1016/j.ijheatmasstransfer.2015.12.074>.
- R. Merle and J. Dolbow. Solving thermal and phase change problems with the eXtended finite element method. *Computational Mechanics*, 28(5):339–350, 2002. ISSN 01787675. doi:10.1007/s00466-002-0298-y. URL <http://www.springerlink.com/index/RN9AG3XN8E8QHK5.pdf>.
- H. Ji, D.L. Chopp, and J. Dolbow. A hybrid extended finite element/level set method for modeling phase transformations. *International Journal For Numerical Methods in Engineering*, 54:1209–1233, 2002. URL <http://www3.interscience.wiley.com/journal/93518898/abstract>.
- Min He, Qing Yang, Ning Li, Xiaopeng Feng, and Naifei Liu. An Extended Finite Element Method for Heat Transfer with Phase Change in Frozen Soil. *Soil Mechanics and Foundation Engineering*, 57(6):497–505, 2021. ISSN 15739279. doi:10.1007/s11204-021-09698-z.

- I. Babuska and A.K. Aziz. On the angle condition in the finite element method. *SIAM Journal on Numerical Analysis*, 13:214–226, 1976. doi:<https://doi.org/10.1137/0713021>.
- J. Shewchuk. What is a good linear finite element? interpolation, conditioning, anisotropy, and quality measures (preprint). *University of California at Berkeley*, 73:137, 2002.
- A. Hannukainen, S. Korotov, and M. Křížek. The maximum angle condition is not necessary for convergence of the finite element method. *Numerische Mathematik*, 120(1-6):79–88, 2012a. ISSN 0029599X. doi:10.1007/s00211-011-0403-2.
- A. Hannukainen, S. Korotov, and M. Křížek. The maximum angle condition is not necessary for convergence of the finite element method. *Numerische mathematik*, 120(1):79–88, 2012b.
- V. Kučera. On necessary and sufficient conditions for finite element convergence, 2016. URL <http://arxiv.org/abs/1601.02942>.
- M. Duprez, V. Lleras, and A. Lozinski. Finite element method with local damage of the mesh. *ESAIM: Mathematical modelling and numerical analysis*, 53:1–10, 2019.
- Horatio Scott Carslaw and John Conrad Jaeger. *Conduction of heat in solids*. Clarendon Press, 1959.